PHILOSOPHICAL TRANSACTIONS OF THE ROYAL SOCIETY B

Phil. Trans. R. Soc. B (2007) **362**, 1393–1406
doi:10.1098/rstb.2007.2123
Published online 20 June 2007

Fluid–structure interaction models of the mitral valve: function in normal and pathological states

K. S. Kunzelman[1,*], D. R. Einstein[2] and R. P. Cochran[1]

[1]*Central Maine Medical Center, 60 High Street, Lewiston, ME 04210, USA*
[2]*Pacific Northwest National Laboratory, Richland, WA 99352, USA*

Successful mitral valve repair is dependent upon a full understanding of normal and abnormal mitral valve anatomy and function. Computational analysis is one such method that can be applied to simulate mitral valve function in order to analyse the roles of individual components and evaluate proposed surgical repair. We developed the first three-dimensional finite element computer model of the mitral valve including leaflets and chordae tendineae; however, one critical aspect that has been missing until the last few years was the evaluation of fluid flow, as coupled to the function of the mitral valve structure. We present here our latest results for normal function and specific pathological changes using a fluid–structure interaction model. Normal valve function was first assessed, followed by pathological material changes in collagen fibre volume fraction, fibre stiffness, fibre splay and isotropic stiffness. Leaflet and chordal stress and strain and papillary muscle force were determined. In addition, transmitral flow, time to leaflet closure and heart valve sound were assessed. Model predictions in the normal state agreed well with a wide range of available *in vivo* and *in vitro* data. Further, pathological material changes that preserved the anisotropy of the valve leaflets were found to preserve valve function. By contrast, material changes that altered the anisotropy of the valve were found to profoundly alter valve function. The addition of blood flow and an experimentally driven microstructural description of mitral tissue represent significant advances in computational studies of the mitral valve, which allow further insight to be gained. This work is another building block in the foundation of a computational framework to aid in the refinement and development of a truly non-invasive diagnostic evaluation of the mitral valve. Ultimately, it represents the basis for simulation of surgical repair of pathological valves in a clinical and educational setting.

Keywords: mitral valve; FSI model; computer model; fluid flow

1. INTRODUCTION

Since the development of cardiopulmonary bypass, open heart surgery has been the definitive treatment for mitral regurgitation, extending longevity and improving quality of life in hundreds of thousands of patients annually. Mitral valve repair is considered superior to mitral valve replacement owing to lower operative mortality, improved late survival, a reduced risk of endocarditis, fewer thromboembolic complications and better preservation of left ventricular function (Yun & Miller 1991; Enriquez-Sarano *et al.* 1995; Gillinov 1998; Jamieson *et al.* 1999; Grossi 2001; Cohn 2002).

Successful mitral valve repair is dependent upon a full understanding of normal and abnormal mitral valve anatomy and function. The functional components of the mitral valve include the left atrial wall, the annulus, the leaflets, the chordae tendineae, the papillary muscles and segments of the left ventricular myocardium (Brock 1952; Rusted *et al.* 1952; Roberts 1983; figure 1). Abnormal anatomy or function of any one of these components can result in valvular dysfunction (Perloff & Roberts 1972). Much of our knowledge of abnormal mitral valve function is based on surgical and post-mortem studies (Waller *et al.* 1982; Olson *et al.* 1987). While these studies are quantitative in some cases, they are limited by evaluation of valve anatomy in a fixed and non-functioning state. A more sophisticated analysis method is necessary to gain a full understanding of mitral valve function. Computational analysis is one such method that can be applied to simulate mitral valve function in order to analyse the roles of individual components. However, very few groups have successfully developed models for structural analysis of the mitral valve.

(a) *Mathematical analysis*

Early on, several groups attempted to model mitral valve anatomy and function mathematically. These models were limited to two dimensions, i.e. a cross section was taken through the midline of the anterior and posterior leaflets (Ghista & Rao 1972; Arts *et al.* 1983). Numerical formulae have been applied to model the leaflet shapes, but significant assumptions were required to apply the mathematical models. These included assuming identical shapes for the anterior and posterior leaflets, or assuming the leaflet curvature to be of specific geometric shape (ellipse, cylinder, etc.). Such assumptions are anatomically incorrect and the results of these studies are not consistent with physiologic observations (Priola *et al.* 1970; Pohost 1975;

* Author for correspondence (kunzelka@cmhc.org).

One contribution of 21 to a Theme Issue 'Bioengineering the heart'.

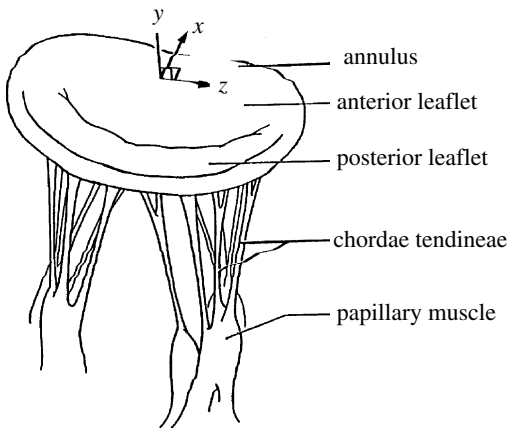

Figure 1. Mitral valve structure, including annulus, leaflets, chordae tendineae and papillary muscles.

Rubenstein *et al.* 1975). More sophisticated mathematical models were computer-aided, but were initially limited to two dimensions, assumed elliptical leaflet shapes and did not employ finite element (FE) analysis (Hunter *et al.* 1983; Miller & Marcotte 1987).

(b) *Finite element analysis*

We developed the first three-dimensional FE computer model of the mitral valve including leaflets and chordae tendineae to analyse the deformation and stress patterns under systolic loading conditions. Our FE model includes all the essential anatomic components, average tissue thickness, orientation of collagen fibres throughout the valve and related orthotropic mechanical properties of leaflet and chordal tissues (Kunzelman *et al.* 1993). The results of our studies have correlated well with published physiologic data (Salisbury *et al.* 1963; Clark 1973; Lim & Boughner 1977; Arts *et al.* 1983). In addition to analysis of normal valves (Kunzelman 1991; Kunzelman *et al.* 1993), we have also simulated pathologically altered valves (Reimink *et al.* 1995, 1996; Kunzelman *et al.* 1996, 1997; Quick *et al.* 1997; Kunzelman & Cochran 1999) and valves that have undergone surgical repair (Reimink *et al.* 1995, 1996; Kunzelman *et al.* 1996, 1998*a*; Kunzelman & Cochran 1999; table 1).

After completion of the normal model, we first examined 'conformational' pathological changes to the structure of the valve and appropriate surgical repair for each pathology. We first examined posterior dilatation, a common pathological finding. When compared with the normal model, with posterior annular dilation (Kunzelman *et al.* 1997), stresses were increased more than 100% in both anterior and posterior leaflets, and even more so in the chordae. Coaptation was delayed and the leaflets never fully coapted. Simulation of flexible and rigid ring annuloplasty to correct dilatation (Kunzelman *et al.* 1998*a*) showed reduced stresses and improved coaptation relative to annular dilatation. Next, simulation of a perforation in the anterior leaflet (Kunzelman 1991) showed stress concentrations that could lead to further tearing. Patching of anterior leaflet perforation (Kunzelman 1991) demonstrated that stress concentrations were eliminated and leaflet stress was returned to normal. Subsequently, another common pathological finding that requires surgical intervention, anterior and posterior chordal rupture, was simulated in several models (Reimink *et al.* 1995, 1996; Kunzelman *et al.* 1996). It was shown that stresses were severely elevated in adjacent chords, which may lead to further elongation or rupture, while in its most severe form, papillary muscle rupture (Kunzelman 1991) resulted in complete leaflet flail. Finally, simulation of extended polytetrafluoroethylene (ePTFE) suture for chordal replacement (Reimink *et al.* 1995, 1996; Kunzelman *et al.* 1996) showed that the length of the suture replacement was more important than size in terms of normalizing chordal and leaflet stresses.

Table 1. Types of mitral valve pathology and repair simulated.

	pathology	repair
type I	annular dilatation	ring annuloplasty
	leaflet perforation	pericardial patch replacement
type II	chordal rupture	chordal replacement
	papillary muscle rupture	
type IIIa	leaflet thickening, stiffening	hemi-homograft replacement
type IIIb	papillary displacement (ischremic dysfunction)	

In other pathological conditions, the microstructure of mitral valve tissue is altered in response to stress (Quick *et al.* 1997, 2004; Kunzelman *et al.* 1998*b*), resulting in changes in tissue thickness, stiffness or both. In our model simulations of such changes (Kunzelman *et al.* 1998*b*), increased tissue stiffness resulted in increased leaflet and chordal stresses, as well as reduced coaptation. Increased tissue thickness reduced not only leaflet and chordal stresses, but also coaptation. In some cases, where the changes in the valve microstructure affect only a part of the valve, replacement with partial homograft is an option. When we examined the effect of 'hemi-homograft' replacement (Kunzelman & Cochran 1999), we found that while coaptation is restored, asymmetry may result due to mismatched leaflet properties and that ring annuloplasty may also be necessary.

Finally, one of the more elusive problems in cardiac surgery, mitral ischaemic dysfunction, was modelled by moving the physical location of the posteromedial papillary muscle progressively outward, to simulate a ventricular infarct involving the papillary muscle (Cochran & Kunzelman 1998). Stress increases were seen in all components of the valve, with an asymmetric pattern, and were greatest near the free edge of the posterior leaflet. In addition, the leaflets were restricted from closing completely, allowing regurgitation.

Only recently, several other groups have developed three-dimensional FE models of the mitral valve. Salgo *et al.* (2002) presented a model of the leaflets only to assess the effect of annular shape on leaflet curvature and stress. Lim *et al.* (2005) published a model of the leaflets and chordae, and performed a quasi-static analysis of leaflet stress and the relationship to asymmetry. Alfieri's group developed a model of leaflets and chordae to assess a new 'dog-bone' ring prosthesis (Maisano *et al.* 2005). For these three models, differing

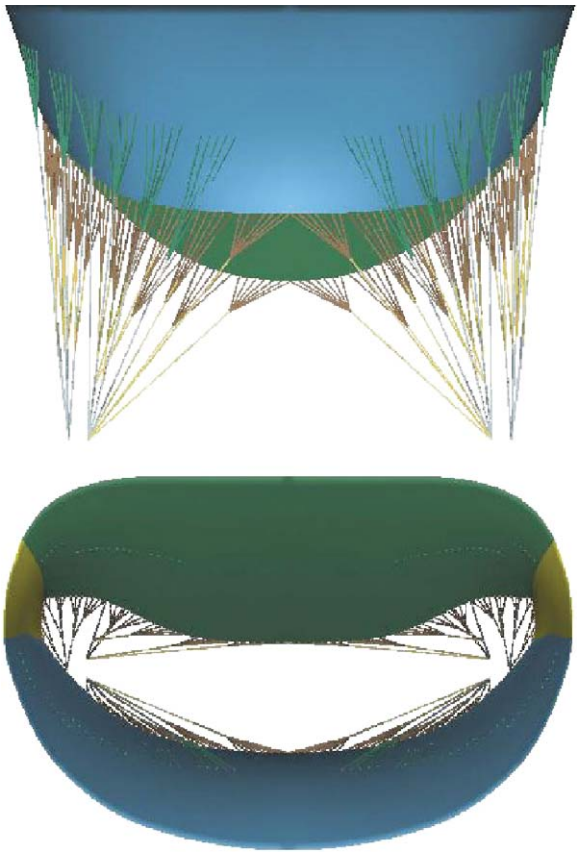

Figure 2. Geometry of mechanical model: leaflets, commissures, branched chords and multiple papillary insertions.

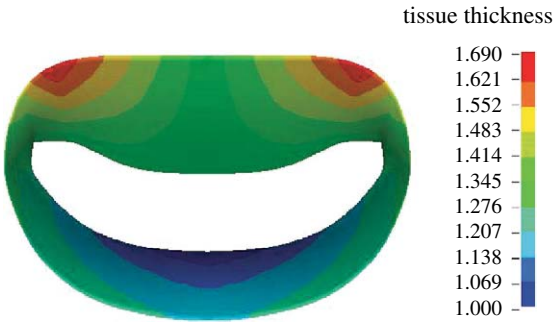

Figure 3. Distribution of leaflet thickness.

methods of determining initial leaflet shape were used, and the similarity to actual valve geometry is variable. The limitations of these models are that they assumed constant leaflet thickness, used non-linear isotropic material models and did not include fluid flow.

One of the more exciting and controversial techniques in mitral valve repair, the Alfieri 'edge-to-edge' approximation, has recently been simulated by several groups. Computational haemodynamic models from Alfieri's group used a fixed geometry for the leaflets, atrium and ventricle, and assessed fluid flow (Maisano *et al.* 1999; Redaelli *et al.* 2001), and a separate static structural model assessed diastolic pressure loading on the leaflets (Votta *et al.* 2002). Another group from Italy recently assessed edge-to-edge repair as well, using sequential models of the leaflets and then leaflets and chordae, beginning with linear elastic properties and ending with hyperelastic properties (Dal Pan *et al.* 2005). All these models demonstrated altered stress

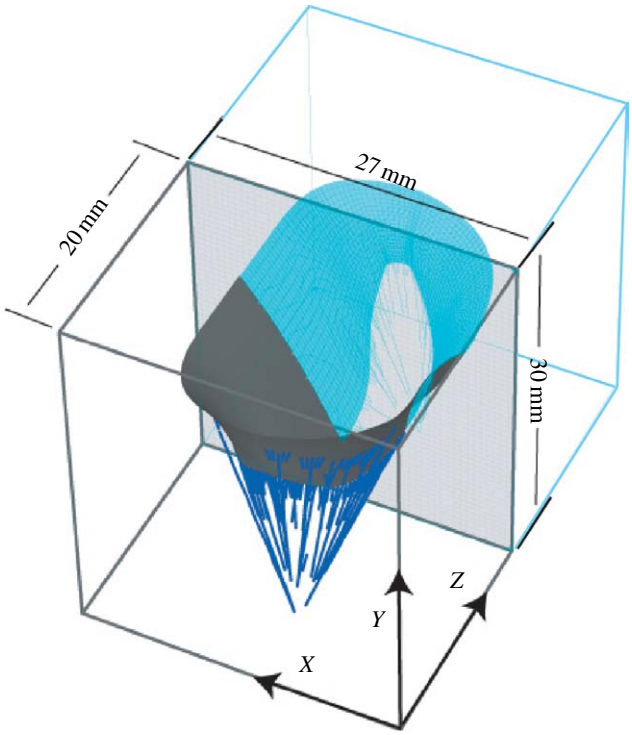

Figure 4. Mitral geometry, symmetry conditions and dimensions of fluid domain.

distributions or altered fluid flow with the edge-to-edge repair technique. However, interpretation of the results is limited by assumptions related to geometry (constant tissue thickness or non-branched chordae) and material properties (linear or isotropic non-linear), and none have coupled fluid flow to mechanical function of the leaflets.

(c) *Fluid–structure interaction models*

In recent years, we have begun to address the critical area of fluid–structure interaction (FSI) and have continued to develop our model of the mitral valve. We are now addressing the evaluation of fluid flow, as coupled to the function of the mitral valve structure. To date, the coupled FSI mitral model that we have presented is the only such model that we are aware of (Einstein *et al.* 2004, 2005*a*,*b*). Our model includes non-constant tissue thickness, anisotropic non-linear material properties specific for each leaflet based on collagen fibre orientation and branched chordae tendineae. Using this model, we have analysed the effect of diseased tissue properties. Our current model of the mitral valve provides a unique opportunity to assess both the mechanical effect of repair techniques, as well as the effect on fluid flow, in both the diastolic and the systolic phase, in the setting of mitral valve pathology. Detailed models of this type are necessary to more fully understand the function of the mitral valve in normal, diseased and surgically repaired states. We present here our latest results for normal function and specific pathological changes using the FSI model.

2. MATERIAL AND METHODS

The commercial FE program, LS-DYNA (Livermore Software Technology Corporation, Livermore, CA), was used to perform all simulations. LS-DYNA is a transient hydrocode,

typically applied to high-speed compressible flows. Custom subroutines to describe the non-linear anisotropic behaviour of mitral tissue were added and have been previously described (Einstein *et al.* 2003).

(a) *Model geometry*

The mid-diastolic surface geometry of the mitral valve leaflets and papillary muscle tips as well as the number and radiation pattern of the chordae tendineae were developed from fresh porcine hearts (Kunzelman *et al.* 1993; figure 2). Regionally varying thicknesses were assigned to the anterior and posterior leaflets (figure 3). Twelve branched chordae radiate from three heads representing the anterior papillary tip.

Dynamic video fluoroscopic data suggest that the mitral annulus is approximately symmetric about the septal–lateral midline (Komeda *et al.* 1996; Dagum *et al.* 2000). It is recognized that asymmetry exists with regard to subvalvular geometry and motion, particularly in pathological conditions including ischaemic dysfunction (Komeda *et al.* 1996, 1997; Dagum *et al.* 2000). Nevertheless, we initially chose to construct a model that is symmetric about the midline plane for computational efficiency. The valve geometry was immersed in a regular fluid domain appropriate for *in vitro* verification (figure 4).

(i) *Pressure loads*

Atrial and ventricular pressure load curves were applied to the atrial and ventricular surfaces of the fluid domain (figure 5). Both curves are based on porcine *in vivo* measurements made with a Millar MIKRO-TIP catheter (Millar Instruments, Inc., Houston, TX) in our laboratory. Pressure crossover occurred at 0.032 s from the beginning of simulation.

(b) *Leaflets*

As the bending behaviour of mitral leaflet tissue has never been quantified, we assumed that the leaflets act as membranes. In other words, curvatures do not produce moments. The FORTRAN code for this membrane formulation is fully described by Einstein *et al.* (2003). Mean collagen fibre angles were mapped to both anterior and posterior leaflets from previously acquired small-angle light-scattering (SALS) data (Cochran *et al.* 1991). The anterior and posterior leaflets were discretized into 740 elements each. The commissure was modelled with 180 elements. Both leaflets and the commissure elements were coupled to the fluid.

Mitral leaflet tissue material behaviour is characterized as an oriented entangled population of crimped collagen fibres embedded in an isotropic phase of gel-like glycoproteins and a network of isotropic elastin (figure 6). Mathematically, the stress–strain behaviour (figure 7) of the mitral leaflets was characterized by the following structural constitutive equation:

$$\boldsymbol{S} = p\mathcal{J}\boldsymbol{C}^{-1} + 2\mathcal{J}^{-2/3}\mathrm{DEV}\left[\frac{\partial \tilde{W}}{\partial \tilde{\boldsymbol{C}}}\right],$$

$$\frac{\partial \tilde{W}}{\partial \tilde{\boldsymbol{C}}} = \alpha \boldsymbol{I} + \int_{-\pi/2}^{\pi/2} S_{\mathrm{f}} R(\theta) \mathsf{A} \otimes \mathsf{A}\, \mathrm{d}\theta,$$

$$S_{\mathrm{f}} = A\left[\exp\left[\frac{B}{2}(\mathsf{A}(\theta)\boldsymbol{C}\mathsf{A}(\theta) - 1)\right] - 1\right],$$

$$R(\theta) = \frac{1}{\sigma\sqrt{2\pi}} \exp\left[\frac{-(\theta-\mu)^2}{2\sigma^2}\right],$$

where $\boldsymbol{S}$ is the second Piola–Kirchhoff stress; $\boldsymbol{C}$ is the right-Cauchy deformation; p is the pressure; $\mathcal{J}$ is the Jacobian or volume ratio; S_{f} is the collagen stress/strain behaviour; $\boldsymbol{I}$ is the identity matrix and A is the orientation tensor. μ is the mean fibre direction, and the Gaussian, $R(\theta)$, relates to the distribution of collagen fibres in the plane of the tissue and has been determined directly by SALS (Cochran *et al.* 1991). A, B, σ and α are material parameters derived from fitting the structural constitutive equation to published biaxial data for mitral valve anterior and posterior leaflet (May-Newman & Yin 1998), and these can be varied to simulate pathological changes. A relates to the volume fraction of collagen and B relates to the stiffness of an equivalent fibre that subsumes the idea of recruitment into an exponential. σ is a statistical parameter representative of fibre splay. The isotropic term α relates to stiffness of the matrix, which is dependent upon the quasi-linear elastic behaviour of both elastin (which primarily supports tension) and the hydrated admixture of proteins and glycoproteins (which primarily support compression). Greater detail is given in Einstein *et al.* (2003). Normal material parameters for both anterior and posterior leaflet are given in table 2. The density is set to 1.04×10^{-6} kg mm^{-3} and the bulk modulus to 2.5×10^{4} kPa for all mitral tissue.

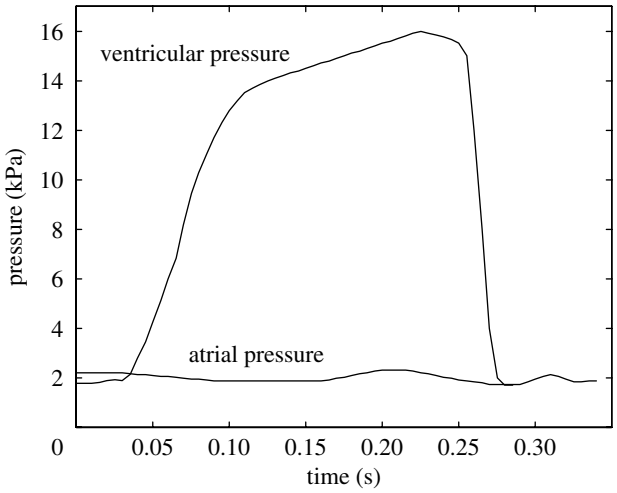

Figure 5. Atrial (lower) and ventricular (upper) pressure profiles applied to the top and bottom of the fluid domain.

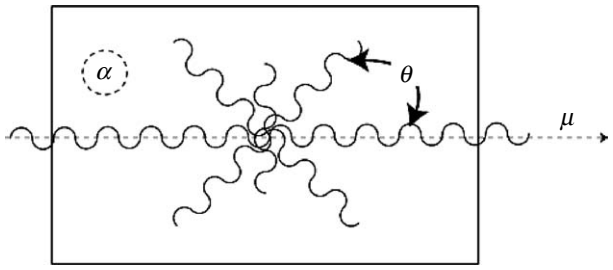

Figure 6. Structural paradigm for mitral leaflet tissue. Collagen fibres (wavy lines) are embedded in an isotropic matrix (α). Locally, the fibres have a mean preferred direction (μ). The standard deviation (σ) determines the Gaussian distribution of collagen fibres about that mean as a function of the splay angle (θ).

(c) *Chordae*

The chordae were modelled as tension-only cables. Though it is widely believed that the chordae act as secondary orifices for blood flow, they are not coupled to the fluid. Chordal diameters are given in table 3. The stress/strain behaviour of the chordae tendineae, like that of the mitral leaflet tissue, is non-linear. As chordae are uniaxial, experimental data are

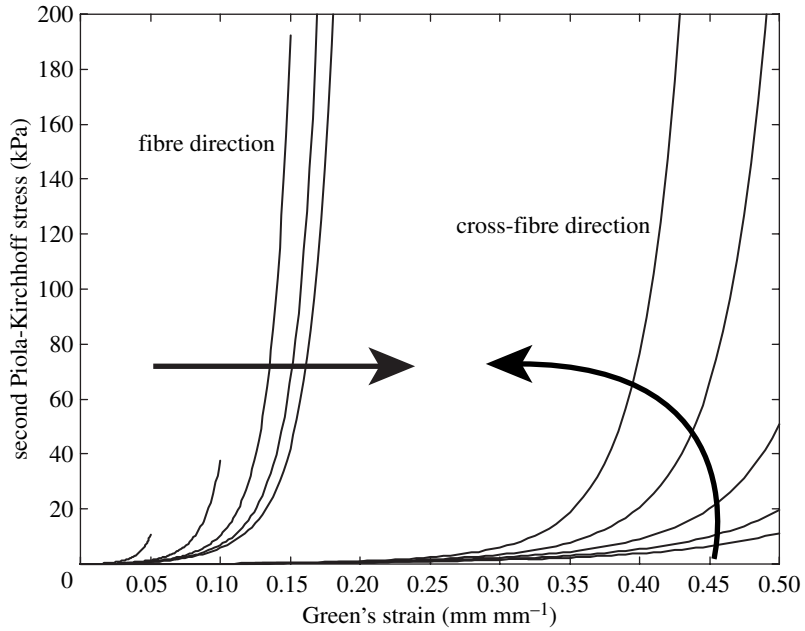

Figure 7. Anterior mitral valve stress–strain behaviour, fibre and cross-fibre directions. Arrows indicate the effect of increasing strain levels in the orthogonal direction.

Table 2. Normal leaflet material parameters.

normal	A (kPa)	B	σ (°)	α (kPa)
anterior	0.070	40	20	10
posterior	0.005	40	20	10
commissure	0.030	40	20	10

Table 3. Chordal geometric properties.

	cross section (mm^2)
strut chord	1.15
primary basal	0.79
subbasal	0.23
primary marginal	0.45
submarginal	0.15

directly input for chordae material behaviour. Chordal stress/strain data were digitized from our published data (Kunzelman & Cochran 1990; table 4).

(d) *Blood*

A Eulerian formulation was used to model the blood domain. Blood was modelled as a compressible, Newtonian fluid. Specifically, the deviatoric stress depends linearly on the shear rate, while compressibility is governed by the equation of state

$$P - P_0 = K(\mathcal{J} - 1),$$

where P is the pressure, K is the blood bulk modulus and $\mathcal{J}$ is the Jacobian or volume ratio. For computational efficiency, the bulk modulus was lowered to 2.5×10^4 kPa from an estimated value of 1.0×10^7 kPa (Masugata *et al.* 1998). Blood viscosity was determined from published data collected in a cone-in-plate viscometer at 37°C and a shear rate of 180 s^{-1} (Stein & Sabbah 1978). An average non-anaemic value of 0.045 P (kg mm^{-1} s) was adopted. Density was set to 1.00×10^{-6} kg mm^{-3}. Grid density for the fluid domain was $35\times53\times48$ fluid elements. (An investigation of grid sensitivity was performed, and increased fluid grid density beyond these ultimately chosen values did not further improve solution results.) Boundary conditions were such that the membrane was pinned on its edges, and the fluid boundary was fixed in displacement and rotation on four sides. At the bottom of the fluid 'box', below the membrane, a pressure was applied to the fluid faces. The pressure was ramped from 0 to 12 kPa (100 mmHg) in 0.05 s and held constant at 12 kPa until the end of the simulation at 0.2 s. The top face of the fluid domain was free in the vertical direction to permit flow to infinity. Flow was only allowed through the valve orifice, i.e. flow 'around' the exterior annular boundary of the valve was prohibited by the addition of a wetted rigid membrane between the annulus and exterior of the fluid domain.

Table 4. Leaflet material parameters for pathological alterations.

normal	A (kPa)	B	σ (°)	α (kPa)
anterior	0.070	40	20	10
posterior	0.005	40	20	10
commissure	0.030	40	20	10
volume fraction (A)				
$A=A/10$	$A/10$	40	20	10
$A=A\times10$	$A\times10$	40	20	10
fibre stiffness (B)				
$B=35$	A	35	20	10
$B=45$	A	45	20	10
fibre splay (σ)				
$\sigma=10$	A	40	10	10
$\sigma=30$	A	40	30	10
isotropic phase (α)				
$\alpha=1$	A	40	20	1
$\alpha=100$	A	40	20	100
$\alpha=1000$	A	40	20	1000

(e) *Coupling algorithm*

The coupling algorithm is an interface-capturing rather than interface-tracking approach. The Eulerian domain of the fluid (blood) and the Lagrangian domain of the structures (leaflets and chordae) overlap. Though they are topologically independent, momentum is passed back and forth between

them. Theoretically, the equation of motion of the wetted Lagrangian surface and of the neighbouring Eulerian fluid must be solved for monolithically. In contrast, we stagger the interaction by one time step. However, the maximum time-step criterion for explicit integration implies that the time step is small enough to capture a sound wave travelling across the smallest element. Thus, the error is limited. To effect the exchange of momentum, the nodes of the Lagrangian shells interact as boundary nodes with the fluid. The Lagrangian mesh is advanced one time step. The boundary nodes are then used as boundary conditions to the Eulerian fluid elements, which react by altering their velocity and pressure. These are then treated as boundary constraints on the Lagrangian structure at the next time step.

More specifically, all the fluid elements containing a structural node are identified. The structural nodal mass is then distributed to the fluid element nodes as

$$m_i^{\text{fluid}} = m_i^{\text{fluid}} + h_i \cdot m^{\text{structure}},$$

where i is the nodal index and h is a weighting coefficient. The structural nodal force is also distributed to the fluid as

$$F_i^{\text{fluid}} = F_i^{\text{fluid}} + h_i \cdot F^{\text{structure}}.$$

The new fluid nodal acceleration becomes

$$a_i^{\text{fluid}} = \frac{F_i^{\text{fluid}}}{m_i^{\text{fluid}}}.$$

The structural nodal acceleration is then constrained or matched to the fluid elemental acceleration as

$$a_i^{\text{structure}} = \sum_{i=1}^{8} h_i \cdot a_i^{\text{fluid}}.$$

In addition, the structural nodal momentum is distributed to the fluid element nodes as

$$M_i^{\text{fluid}} = M_i^{\text{fluid}} + h_i \cdot M^{\text{structure}}.$$

The new fluid nodal velocity becomes

$$u_i^{\text{fluid}} = \frac{M_i^{\text{fluid}}}{m_i^{\text{fluid}}}.$$

Finally, the structural nodal velocity is constrained to the fluid velocity as

$$u_i^{\text{structure}} = \sum_{i=1}^{8} h_i \cdot u_i^{\text{fluid}}.$$

(f) *Pathological alterations*

We further used our model to assess alteration of micro-structural components, as seen in diseased tissue (Einstein *et al.* 2005). Specifically, we examined the effects of perturbations on material constants A, B, σ and α. Parameter A may be considered to be proportional to the volume fraction of effective collagen fibres. A was increased and then decreased by a factor of 10 (relative to each leaflet and the chordae). Parameter B governs the stiffness of individual effective fibres and was decreased to 35 and then increased to 45. The fibre splay parameter σ, or the degree of local fibre alignment, was decreased to 10° and then increased to 30°. The isotropic parameter α was decreased to 1 kPa and increased to 100 and 1000 kPa.

(g) *Assessment*

Stress and strain in the leaflets and chords were assessed. Papillary muscle force was determined as the sum of the reaction forces on the three nodes that represented the three heads of the anterolateral papillary muscle. In addition, transmitral flow (defined in such a way that negative flow is towards the atrium and positive flow towards the ventricle) and time to leaflet closure were assessed. Finally, to assess acoustic radiation (heart valve sound), the sampled and filtered average pressure signal from the computational model was analysed in the time–frequency plane with a Wigner–Ville distribution and a radially Gaussian kernel. (Results for the frequency analysis are given here for the normal model only.)

3. RESULTS

(a) *Normal model*

(i) *Stress and strain*

Late diastolic and early systolic peak principle stress occurred in the trigone of the anterior leaflet (figure 8). By 0.047 s at a transvalvular pressure (left ventricular pressure minus left atrial pressure) of 11.8 mmHg, the valve was mostly closed and the peak principle stress extended from the strut chordae to the trigones. At 0.070 s, the valve was fully closed and oscillating. In other words, the fluid is decelerated and cannot pass through the closed orifice. However, both the blood and the tissue possess momentum. This momentum is first converted to strain energy in the tissue, then returned as an acceleration to the fluid, then returned as strain energy again, until the energy of the system decays to steady state. It is these oscillations that are responsible for the first heart sound. The *appearance* of space between the leaflet is an artefact of the graphics, since only the midsurface of the leaflet is shown; thus, the apparent 'gap' is in fact filled by the thickness of the leaflets. Closure is verified by checking the status of the contact elements. The peak stress was 140 kPa and the location was transitioned to the belly of the leaflet and at the insertion of the strut chorda. This corresponded to a transvalvular pressure of 48.0 mmHg. By 0.093 s and a transvalvular pressure of 75.4 mmHg, the stress had risen to 224 kPa and the stress pattern was stable. At the final transvalvular pressure of 98 mmHg at 0.14 s, the stress levelled off to 254 kPa. Circumferential Almansi strains (figure 9) were highly negative on both leaflets towards the commissures and, particularly, in the neighbourhood of the physiological wrinkles ranging from 0.17 to −0.51. Radial Almansi strains, however, were entirely tensile, ranging from 0.04 to 0.25.

(ii) *Papillary muscle force*

The time course of papillary muscle force closely followed the left ventricular pressure curve (figure 10), with a maximum of 2.6 N at a transvalvular pressure of 95 mmHg. A notch in the papillary force curve at approximately 0.06 s from the beginning of simulation corresponded to the onset of coaptation and valvular vibration. Maximum tension in the strut chord was found to be 0.52 N.

(iii) *Flow*

Peak closing flow was 51 ml s^{-1} (figure 11). Regurgitant closing volume, the time integral of transmitral closing flow, was 1.17 ml per beat. Peak backward velocity into the atrium was 886.9 mm s^{-1}. The sequence shown in figure 12 illustrates the development of flow during closure. Where stream-traces appear to penetrate the leaflets, the leaflets are moving with the local fluid velocity. The chordae are not shown

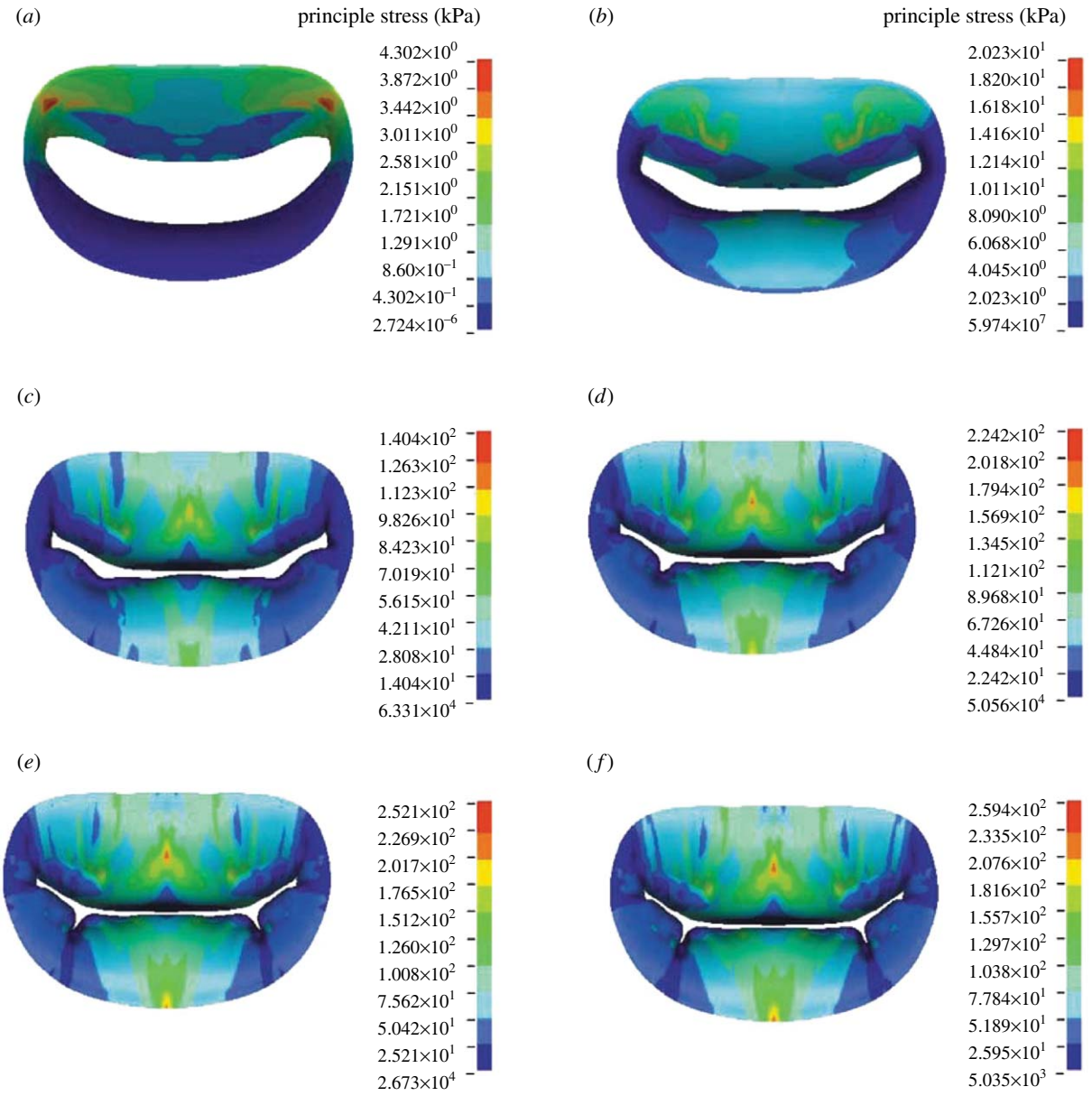

Figure 8. Time course of principle stress in the anterior and posterior leaflets in the normal model. Time: (*a*) 0.023, (*b*) 0.047, (*c*) 0.070, (*d*) 0.093, (*e*) 0.117 and (*f*) 0.140 s. Red colour denotes the highest stress and dark blue the lowest.

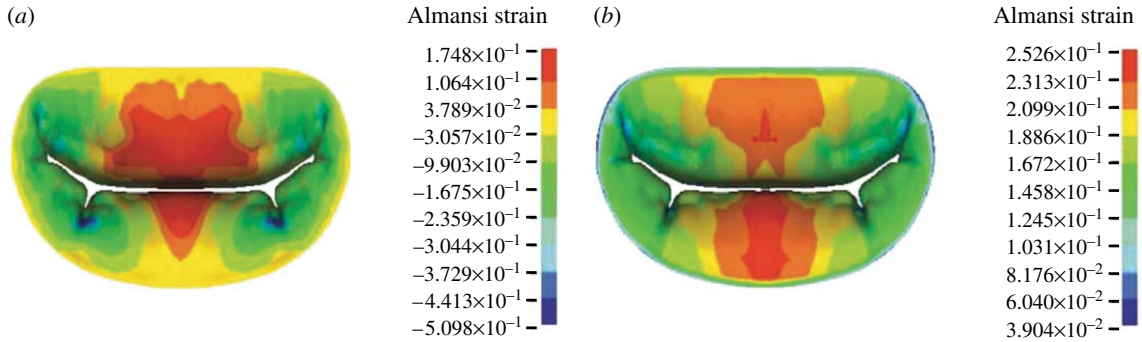

Figure 9. (*a*) Circumferential and (*b*) radial Almansi strains at 0.14 s in normal model. Values with negative numbers are compressive strains.

for the sake of clarity. Though the flow is fully three-dimensional, the stream-traces are plotted on the plane of symmetry to confine them to a two-dimensional plane for more facile interpretation. Note the eddy structures above the mitral valve.

(iv) *Frequency response of S1*

The transformed signal was found to have a downward glide in frequency with a maximum at 72.0 Hz occurring at 0.0604 s from pressure crossover (figure 13). The root mean square of the acoustic

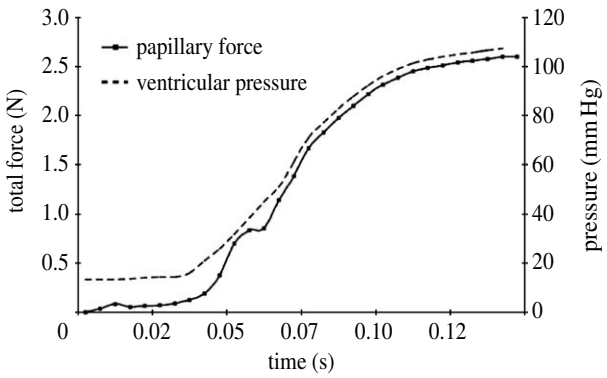

Figure 10. Anterolateral papillary muscle force in normal model.

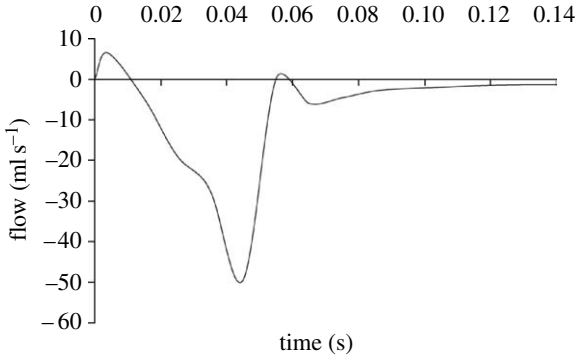

Figure 11. Mitral valve closing flow in normal model.

pressure was 3.3 Pa. This is compared to a typical thoracic S1 recording from sheep in our laboratory. The average maximum peak frequency was 71.7 ± 2.8 Hz and occurred 0.071 ± 0.003 s from the peak of the QRS wave in the ECG.

(b) *Pathological alterations*

(i) *Collagen volume fraction (A)*

Transmitral flow was found to modestly decrease, both when the collagen volume fraction was increased and decreased (figure 14). Interestingly, even in the presence of strong perturbations of the collagen volume fraction, the valve remained competent. The regurgitant volumes for $A = A/10$, A and $10 \times A$ (note that different baseline parameter A values are assigned to anterior and posterior leaflet and commissural zone baseline) were 1.24, 1.17 and 1.04 ml, respectively. The end-of-simulation maximum principle stresses were 234.1, 259.4 and 334.0 kPa, respectively (figure 15).

(ii) *Collagen fibre stiffness (B)*

Transmitral flow was found to modestly decrease, both when the fibre stiffness was increased and decreased (figure 14). Even in the presence of strong perturbations to the fibre stiffness, the valve remained competent. The regurgitant volumes for $B = 35$, 40 and 45 (unitless) were 1.23, 1.17 and 1.02 ml, respectively. The end-of-simulation maximum principle stresses were 332.5, 259.4 and 334.0 kPa, respectively (figure 15).

(iii) *Collagen fibre splay (σ)*

Transmitral flow was found to substantially increase when the fibre splay was decreased to 10° and decrease when the tissue fibre splay was increased to 30° (figure 14). The regurgitant volumes for $\sigma = 10°$, 20° and 30° were 1.67, 1.17 and 1.12 ml, respectively. The end-of-simulation maximum principle stresses were 387.6, 259.4 and 219.7 kPa, respectively (figure 15).

(iv) *Isotropic phase (α)*

Flow was found to vary substantially when α was increased to 100 and 1000 kPa, but did not change substantially when α was decreased to 1 kPa (figure 14). The regurgitant volumes for $\alpha = 1$, 10, 100 and 1000 kPa were 1.21, 1.17, 1.45 and 6.73 ml, respectively. The end-of-simulation maximum principle stresses were 267.5, 259.4, 174.9 and 336.5 kPa, respectively (figure 15).

4. DISCUSSION

We have described the results of a three-dimensional FSI model of the mitral valve that incorporates a continuum representation of mitral leaflet microstructure. Both normal and pathological functions were assessed. Our discussion will focus on the structural and fluid dynamic behaviour of the model, as well as comparing the model predictions to available data.

(a) *Normal model*

(i) *Stress and strain*

The peak principle stress of 254 kPa is 30% lower than the maximum principle stress predicted by earlier models that used linear material properties (Kunzelman *et al.* 1993). Interestingly, both radial and circumferential stresses were tensile for both of the leaflets throughout the simulation, while circumferential Almansi strains were highly compressive on both leaflets towards the commissures and, particularly, in the neighbourhood of the physiological wrinkles. This diametric behaviour of stress and strain has been noted previously in *in vitro* biaxial tests of cardiac tissue (Billiar & Sacks 2000*a*,*b*) and is a fundamental difference between linear and nonlinear behaviour. It is believed that this coupled behaviour is influenced by the fibre splay.

(ii) *Papillary muscle force*

The relationship between papillary muscle force and the left ventricular pressure curve is well documented (Nielsen *et al.* 1999; Jensen *et al.* 2001) with peak values of approximately 2.5 N, corresponding to a maximum transvalvular pressure of approximately 80 mmHg. Our predicted value of 2.6 N agrees quite well with these measurements. The papillary force was found to be distributed unevenly among the basal chords with the chords of the anterior leaflet bearing the greatest load. This is in agreement with previous models (Kunzelman *et al.* 1993; Reimink *et al.* 1996). The strut chord, the thickest of these basal chords, is generally assumed to carry the largest load; this assumption was confirmed in our model. Maximum tension in the strut chord was found to be 0.52 N. An *in vivo* measurement of strut chord tension in dogs found the strut chordal tension to be approximately 0.60 N at 100 mmHg (Salisbury *et al.* 1963).

This measurement is difficult owing to its obviously intrusive nature. Nevertheless, the simulated and measured values are generally in agreement.

(iii) *Flow*
The complex atrial and ventricular flow fields make the *in vivo* quantification of transmitral flow difficult and only semi-quantitative. Nevertheless, the shape of the predicted mitral closing flow is similar to those determined by M-mode echocardiography (Laniado *et al.* 1973, 1975). Closing volume for normal dogs measured by M-mode echocardiography has been reported to be 3.23 ml per beat (Laniado *et al.* 1975). Our predicted closing volume of 1.17 ml is also a small volume, but slightly less. Predicted transmitral flow over time also showed excellent agreement with published *in vitro* transmitral flow data from the Georgia Tech left heart simulator (Jensen *et al.* 2001; figure 16).

(iv) *Acoustic response*
It is now widely recognized that S1 is non-stationary. This feature was observed in both the computational model and the measured thoracic S1 from sheep in our laboratory. The predicted time–frequency signature was found to have a downward glide in frequency with a maximum of 72.0 Hz occurring at 0.060 s from pressure crossover. Similarly, the average maximum peak frequency for the measured thoracic S1 was 71.7 ± 2.8 Hz and occurred 0.071 ± 0.003 s from the peak of the QRS wave in the EKG. Chen *et al.* also found that measured 'intraventricular' S1 was either flat or in the shape of a descending crescent in the time–frequency plane (Chen *et al.* 1997*a–c*), suggesting a qualitative agreement between measured intraventricular S1 and the predicted intraventricular S1.

(b) *Pathological changes*

(i) *Collagen fibre volume fraction (A)*
Preliminary evidence suggests that the equilibrium of mitral leaflet collagen is dynamic, and that the operational longevity of mitral tissue is related to turnover (Quick *et al.* 1997; Dreger *et al.* 2002). It may be that routine remodelling driven by 'contact guidance' (Barocas & Tranquillo 1997) reinforces existent valvular anisotropy by varying the spatial density of leaflet collagen while preserving the underlying spatial orientation of collagen fibre bundles. In other words, it may be that routine remodelling centres on collagen volume fraction. Flow rates across the valve did not vary substantially with decreased and increased volume fraction. Small changes in coaptation times were observed in both the leaflet signals and the acoustic pressure. Peak stresses were higher in the increased volume fraction case but lower in the decreased volume fraction case. However, the stress distribution in both cases was similar to the normal model.

Perturbations to the volume fraction did not alter the pattern of anisotropy of the mitral leaflets and function was preserved. In fact, increased volume fraction led to decreased regurgitant volume. These findings suggest that valvular function is robust to what we have termed *functional proliferation*, i.e. proliferation of the microstructure that preserves the innate mechanical character of the valve leaflets by respecting the purposeful trajectories of mitral collagen bundles.

(ii) *Collagen fibre stiffness (B)*
Unloaded valvular collagen fibre bundles exhibit a characteristic waviness or crimp, the periodicity of which is believed to strongly influence the non-linearity of collagen tension/stretch behaviour and thus the stress/strain behaviour of mitral tissue (Cochran & Kunzelman 1991). The difference in periodicity of basal and marginal chordae, for example, explains the higher stiffness of the latter (Cochran & Kunzelman 1991). Parameter B governs the stiffness of individual effective fibres, and increases and decreases in the fibre stiffness are another example of functional proliferation. Despite profound perturbations to the fibre stiffness, the simulated valve remained competent. Parallel to perturbation of the volume fraction, changes in fibre stiffness did not produce regurgitation. In fact, the transmitral flow was little affected. However, stress was increased considerably both with increased and decreased fibre stiffness.

(iii) *Collagen fibre splay (σ)*
Preliminary evidence suggests that fibre splay, or the degree of local fibre alignment, varies—perhaps functionally—across mitral leaflets (Sacks *et al.* 2002). It is possible to hypothesize that alterations in collagen fibre splay is one of the disease pathways of mitral leaflet tissue. Furthermore, altered fibre splay may account for the disordering of collagen in myxomatous disease and strongly influences the mechanical coupling between deformation along fibre trajectories and the cross-fibre direction. This was manifest in both the quantitative and qualitative difference among principle stress patterns. Increasing the fibre splay created a more uniform distribution of stress in the bellies of anterior and posterior leaflets. Altered anisotropy also notably affected transmitral flow. Decreasing the fibre splay increased the transmitral flow to a value that could be classified as functionally regurgitant and significantly increased the end-of-simulation stress as well. Further, with reduced fibre splay, the peak stresses were shifted to the strut chord as well as to the leaflet margins. The leaflets had more flail in the reduced case and closure was accompanied by notable billowing. The result was a floppy valve with areas of high stress. Furthermore, the floppy leaflets closed later. The anterior closure peak was retarded by nearly 5 ms, while the posterior leaflet closure peak was delayed by almost 10 ms.

(iv) *Isotropic phase (α)*
Both fibrotic proliferation and calcification are pathologies that may lead to an increased leaflet stiffness due to alterations in the isotropic character. In the case of calcification, this isotropic character is due to the mineral having no preferred direction. In the case of fibrosis, it is believed that fibrotic fibrillogenesis has a random—and therefore isotropic—character. By altering the innate anisotropy of the leaflets, isotropic proliferation diminished the closing leaflet velocities, requiring larger pressure gradients for full coaptation.

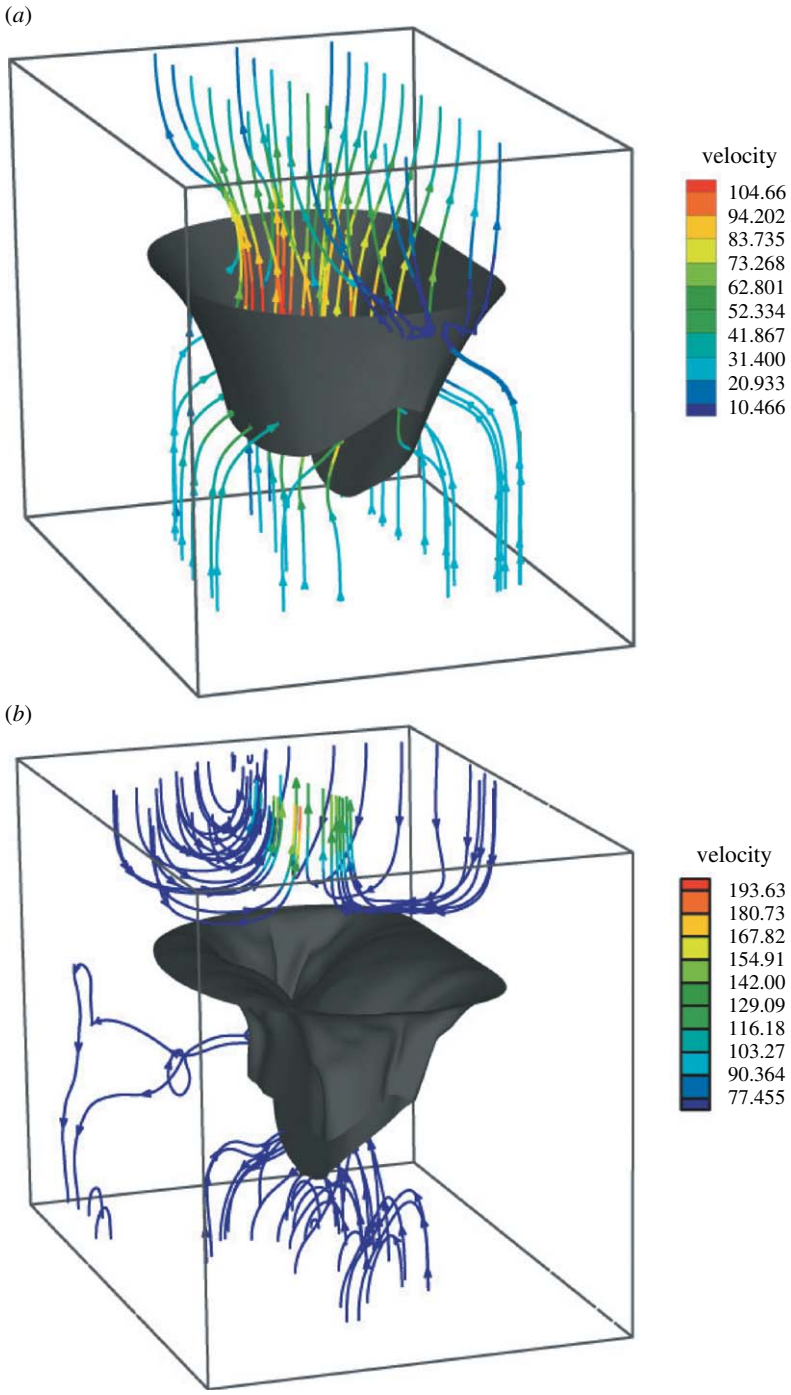

Figure 12. Stream-traces of blood velocity in the (*a*) initial ($t=20$ ms) and (*b*) final ($t=85$ ms) phases of closure in normal model.

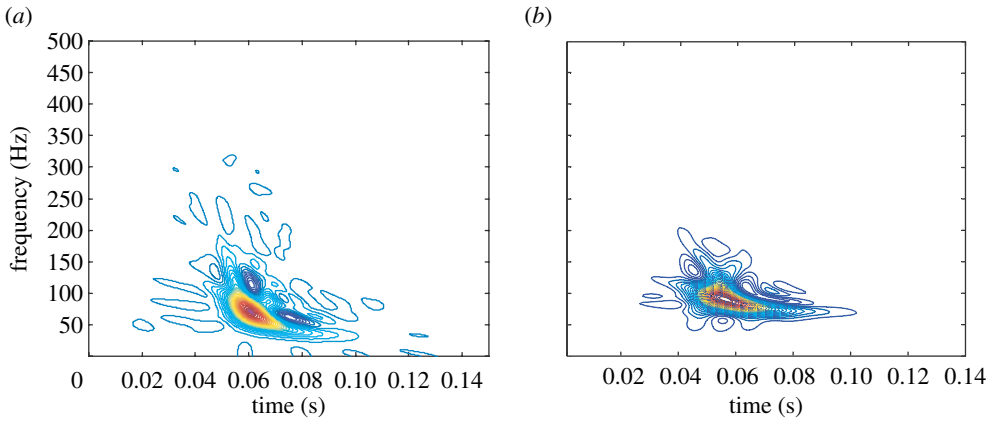

Figure 13. Time–frequency signature of acoustic pressure in (*a*) the FSI model and (*b*) from measured thoracic recordings in sheep (with respect to the onset of systole).

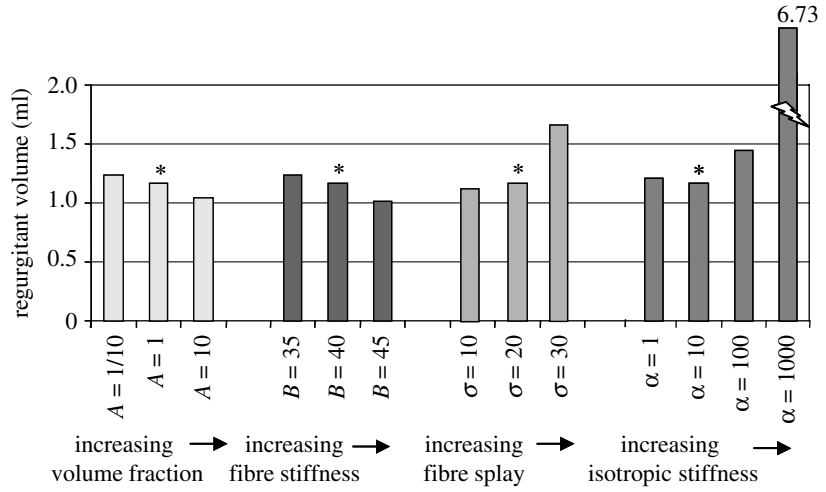

Figure 14. Regurgitant volumes for the models with pathological alterations. Asterisks refer to the normal model.

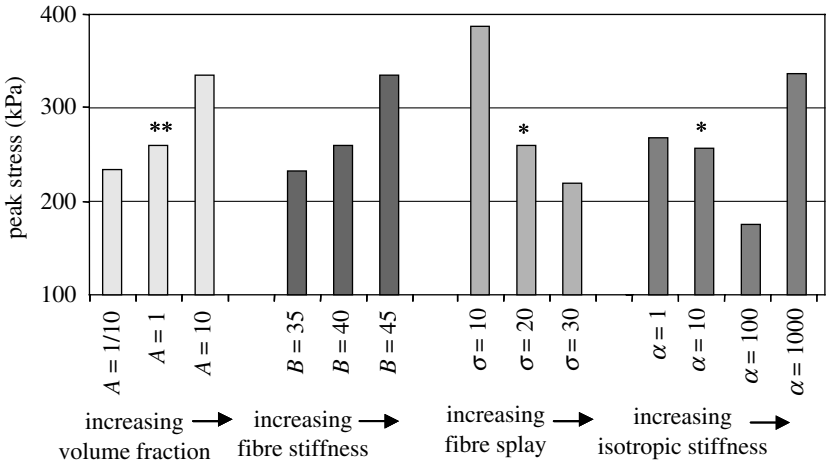

Figure 15. Peak stress for the models with pathological alterations. Asterisks refer to the normal model.

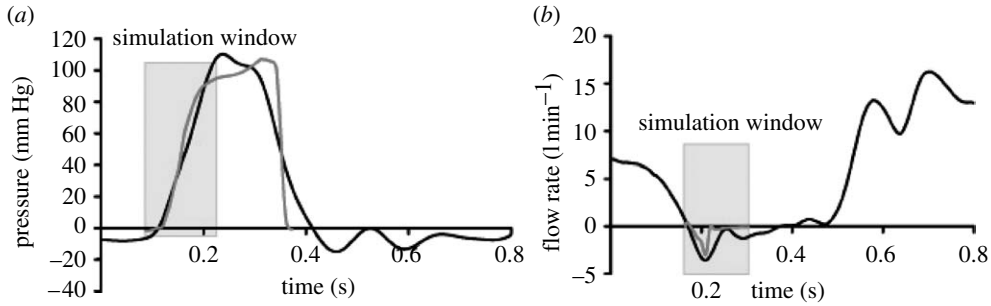

Figure 16. (*a*) Transvalvular pressure and (*b*) transmitral flow: black line, reference (Salisbury *et al.* 1963); grey line, data from computational model. Input transvalvular pressure was shifted to match the early systolic zero crossing in the measured transvalvular pressure. The predicted closing flow (grey line) shows excellent agreement with *in vitro* data (black line) over the simulation window. Note that the predicted flow data were shifted an additional 50 ms to the right due to the inertia-driven lag between pressure and flow in the measured data. (Measured data reprinted with permission from (Jensen *et al.* 2001). © AMBE.)

In addition, increased isotropic stiffness fundamentally altered both the fluid dynamics of transmitral flow and the end-of-simulation stress patterns.

5. CONCLUSION

The more we analyse the mitral valve, the more remarkable it appears in its elegant simplicity and ability to maintain function over a large period of time, range of physiologic states and through various pathological insults. Our initial FE models (without fluid flow) provided insight into normal function, and particular structural pathological changes and surgical correction. The addition of blood flow and an experimentally driven microstructural description of mitral tissue represent significant advances in computational studies of the mitral valve, which allow further insight to be gained. Despite the assumptions that went into this first non-linear fluid–structure coupled model, model predictions closely matched a wide range of

available data. Further, material changes that preserved the anisotropy of the valve leaflets were found to preserve valve function. By contrast, material changes that altered the anisotropy of the valve were found to profoundly alter valve function. Thus, this coupled fluid–structure model constitutes a valid tool for researching the interaction between flow and mitral conformational abnormalities. Furthermore, it is an excellent tool for assessing the functional boundaries between normal and diseased mitral tissue as a function of tissue microstructure. This work is another building block in the foundation of a computational framework to aid in the refinement and development of a truly non-invasive diagnostic evaluation of the mitral valve. Ultimately, it represents the basis for simulation of surgical repair of pathological valves in a clinical and educational setting.

REFERENCES

Arts, T., Meerbaum, S., Reneman, R. & Corday, E. 1983 Stresses in the closed mitral valve: a model study. *J. Biomech.* **16**, 539–547. (doi:10.1016/0021-9290(83)90068-4)

Barocas, V. H. & Tranquillo, R. T. 1997 An anisotropic biphasic theory of tissue-equivalent mechanics: the interplay among cell traction, fibrillar network deformation, fibril alignment, and cell contact guidance. *J. Biomech. Eng.* **119**, 137–145.

Billiar, K. L. & Sacks, M. S. 2000*a* Biaxial mechanical properties of the native and glutaraldehyde-treated aortic valve cusp. Part II: a structural constitutive model. *J. Biomech. Eng.* **122**, 327–335. (doi:10.1115/1.1287158)

Billiar, K. L. & Sacks, M. S. 2000*b* Biaxial mechanical properties of the natural and glutaraldehyde treated aortic valve cusp. Part I: experimental results. *J. Biomech. Eng.* **122**, 23–30. (doi:10.1115/1.429624)

Brock, R. C. 1952 The surgical and pathological anatomy of the mitral valve. *Br. Heart J.* **14**, 489–513.

Chen, D., Durand, L. G., Guo, Z. & Lee, H. C. 1997*a* Time-frequency analysis of the first heart sound. Part 2: an appropriate time-frequency representation technique. *Med. Biol. Eng. Comput.* **35**, 311–317. (doi:10.1007/BF02534082)

Chen, D., Durand, L. G. & Lee, H. C. 1997*b* Time-frequency analysis of the first heart sound. Part 1: simulation and analysis. *Med. Biol. Eng. Comput.* **35**, 306–310. (doi:10.1007/BF02534081)

Chen, D., Durand, L. G., Lee, H. C. & Wieting, D. W. 1997*c* Time-frequency analysis of the first heart sound. Part 3: application to dogs with varying cardiac contractility and to patients with mitral mechanical prosthetic heart valves. *Med. Biol. Eng. Comput.* **35**, 455–461. (doi:10.1007/BF02525523)

Clark, R. E. 1973 Stress–strain characteristics of fresh and frozen human aortic and mitral leaflets and chordae tendineae. Implications for clinical use. *J. Thorac. Cardiovasc. Surg.* **66**, 202–208.

Cochran, R. P. & Kunzelman, K. S. 1991 Comparison of viscoelastic properties of suture versus porcine mitral valve chordae tendineae. *J. Card. Surg.* **6**, 508–513.

Cochran, R. P. & Kunzelman, K. S. 1998 Effect of papillary muscle position on mitral valve function: relationship to homografts. *Ann. Thorac. Surg.* **66**(Suppl. 6), S155–S161. (doi:10.1016/S0003-4975(98)01100-X)

Cochran, R. P., Kunzelman, K. S., Chuong, C. J., Sacks, M. S. & Eberhart, R. C. 1991 Nondestructive analysis of mitral valve collagen fiber orientation. *ASAIO Trans.* **37**, M447–M448.

Cohn, L. H. 2002 Mitral valve repair for ischemic mitral regurgitation. *Adv. Cardiol.* **39**, 153–156.

Dagum, P., Timek, T. A., Green, G. R., Lai, D., Daughters, G. T., Liang, D. H., Hayase, M., Ingels Jr, N. B. & Miller, D. C. 2000 Coordinate-free analysis of mitral valve dynamics in normal and ischemic hearts. *Circulation* **102**(Suppl. 19), III62–III69.

Dal Pan, F., Donzella, G., Fucci, C. & Schreiber, M. 2005 Structural effects of an innovative surgical technique to repair heart valve defects. *J. Biomech.* **38**, 2460–2471. (doi:10.1016/j.jbiomech.2004.10.005)

Dreger, S. A., Taylor, P. M., Allen, S. P. & Yacoub, M. H. 2002 Profile and localization of matrix metalloproteinases (MMPs) and their tissue inhibitors (TIMPs) in human heart valves. *J. Heart Valve Dis.* **11**, 875–880. [discussion 80]

Einstein, D. R., Reinhall, P., Nicosia, M., Cochran, R. P. & Kunzelman, K. 2003 Dynamic finite element implementation of nonlinear, anisotropic hyperelastic biological membranes. *Comput. Methods Biomech. Biomed. Eng.* **6**, 33–44. (doi:10.1080/1025584021000048983)

Einstein, D. R., Kunzelman, K. S., Reinhall, P. G., Cochran, R. P. & Nicosia, M. A. 2004 Haemodynamic determinants of the mitral valve closure sound: a finite element study. *Med. Biol. Eng. Comput.* **42**, 832–846. (doi:10.1007/BF02345218)

Einstein, D. R., Kunzelman, K. S., Reinhall, P. G., Nicosia, M. A. & Cochran, R. P. 2005*a* Non-linear fluid-coupled computational model of the mitral valve. *J. Heart Valve Dis.* **14**, 376–385.

Einstein, D. R., Kunzelman, K. S., Reinhall, P. G., Nicosia, M. A. & Cochran, R. P. 2005*b* The relationship of normal and abnormal microstructural proliferation to the mitral valve closure sound. *J. Biomech. Eng.* **127**, 134–147. (doi:10.1115/1.1835359)

Enriquez-Sarano, M., Schaff, H. V., Orszulak, T. A., Tajik, A. J., Bailey, K. R. & Frye, R. L. 1995 Valve repair improves the outcome of surgery for mitral regurgitation. A multivariate analysis. *Circulation* **91**, 1022–1028.

Ghista, D. N. & Rao, A. P. 1972 Structural mechanics of the mitral valve: stresses sustained by the valve; non-traumatic determination of the stiffness of the *in vivo* valve. *J. Biomech.* **5**, 295–307. (doi:10.1016/0021-9290(72)90046-2)

Gillinov, A. M. *et al.* 1998 Durability of mitral valve repair for degenerative disease. *J. Thorac. Cardiovasc. Surg.* **116**, 734–743. (doi:10.1016/S0022-5223(98)00450-4)

Grossi, E. A. *et al.* 2001 Ischemic mitral valve reconstruction and replacement: comparison of long-term survival and complications. *J. Thorac. Cardiovasc. Surg.* **122**, 1107–1124. (doi:10.1067/mtc.2001.116945)

Hunter, J., Seaton, D., Lively, W., Miller, D. & Stoner, D. 1983 Modelling systolic mitral valve motion: a tool for clarifying mitral prolapse. *Tex. J. Sci.* **35**, 4–36.

Jamieson, W. R., Edwards, F. H., Schwartz, M., Bero, J. W., Clark, R. E. & Grover, F. L. 1999 Risk stratification for cardiac valve replacement. National Cardiac Surgery Database. Database Committee of The Society of Thoracic Surgeons. *Ann. Thorac. Surg.* **67**, 943–951. (doi:10.1016/S0003-4975(99)00175-7)

Jensen, M. O., Fontaine, A. A. & Yoganathan, A. P. 2001 Improved *in vitro* quantification of the force exerted by the papillary muscle on the left ventricular wall: three-dimensional force vector measurement system. *Ann. Biomed. Eng.* **29**, 406–413. (doi:10.1114/1.1366672)

Komeda, M., Glasson, J. R., Bolger, A. F., Daughters II, G. T., Niczyporuk, M. A., Ingels Jr, N. B. & Miller, D. C. 1996 Three-dimensional dynamic geometry of the normal canine mitral annulus and papillary muscles. *Circulation* **94**(Suppl. 9), II159–II163.

Komeda, M., Glasson, J. R., Bolger, A. F., Daughters II, G. T., Ingels Jr, N. B. & Miller, D. C. 1997 Papillary muscle-left ventricular wall 'complex'. *J. Thorac. Cardiovasc. Surg.* **113**, 292–300. (doi:10.1016/S0022-5223(97)70326-X) discussion, pp 300–301.

Kunzelman, K. 1991 Engineering analysis of mitral valve structure and function. Dissertation, University of Texas Southwestern Medical Center, Dallas, TX.

Kunzelman, K. S. & Cochran, R. P. 1990 Mechanical properties of basal and marginal mitral valve chordae tendineae. *ASAIO Trans.* **36**, M405–M408.

Kunzelman, K. & Cochran, R. 1999 Hemi-homograft replacement of the mitral valve: a finite element model. In *Stentless bioprostheses* (eds H. A. Huysmans, T. E. David & S. Westaby), pp. 31–38, 2nd edn. Oxford, UK: Isis Medical Media, Ltd.

Kunzelman, K. S., Cochran, R. P., Chuong, C., Ring, W. S., Verrier, E. D. & Eberhart, R. D. 1993 Finite element analysis of the mitral valve. *J. Heart Valve Dis.* **2**, 326–340.

Kunzelman, K., Reimink, M. S., Verrier, E. D. & Cochran, R. P. 1996 Replacement of mitral valve posterior chordae tendineae with expanded polytetrafluoroethylene suture: a finite element study. *J. Card. Surg.* **11**, 136–145. [discussion 146]

Kunzelman, K. S., Reimink, M. S. & Cochran, R. P. 1997 Annular dilatation increases stress in the mitral valve and delays coaptation: a finite element computer model. *Cardiovasc. Surg.* **5**, 427–434. (doi:10.1016/S0967-2109(97)00045-8)

Kunzelman, K. S., Reimink, M. S. & Cochran, R. P. 1998*a* Flexible versus rigid ring annuloplasty for mitral valve annular dilatation: a finite element model. *J. Heart Valve Dis.* **7**, 108–116.

Kunzelman, K. S., Quick, D. W. & Cochran, R. P. 1998*b* Altered collagen concentration in mitral valve leaflets: biochemical and finite element analysis. *Ann. Thorac. Surg.* **66**(Suppl. 6), S198–S205. (doi:10.1016/S0003-4975(98)01106-0)

Laniado, S., Yellin, E. L., Miller, H. & Frater, R. W. 1973 Temporal relation of the first heart sound to closure of the mitral valve. *Circulation* **47**, 1006–1014.

Laniado, S., Yellin, E., Kotler, M., Levy, L., Stadler, J. & Terdiman, R. 1975 A study of the dynamic relations between the mitral valve echogram and phasic mitral flow. *Circulation* **51**, 104–113.

Lim, K. O. & Boughner, D. R. 1977 Scanning electron microscopical study of human mitral valve chordae tendineae. *Arch. Pathol. Lab. Med.* **101**, 236–238.

Lim, K. H., Yeo, J. H. & Duran, C. M. 2005 Three-dimensional asymmetrical modeling of the mitral valve: a finite element study with dynamic boundaries. *J. Heart Valve Dis.* **14**, 386–392.

Maisano, F., Redaelli, A., Pennati, G., Fumero, R., Torracca, L. & Alfieri, O. 1999 The hemodynamic effects of double-orifice valve repair for mitral regurgitation: a 3D computational model. *Eur. J. Cardiothorac. Surg.* **15**, 419–425. (doi:10.1016/S1010-7940(99)00071-8)

Maisano, F., Redaelli, A., Soncini, M., Votta, E., Arcobasso, L. & Alfieri, O. 2005 An annular prosthesis for the treatment of functional mitral regurgitation: finite element model analysis of a dog bone-shaped ring prosthesis. *Ann. Thorac. Surg.* **79**, 1268–1275. (doi:10.1016/j.athoracsur.2004.04.014)

Masugata, H., Senda, S., Mizushige, K., Lu, X., Kinoshita, A., Sakamoto, H., Nozaki, S., Sakamoto, S. & Matsuo, H. 1998 Mitral valve tissue characterization using acoustic microscopy. *J Cardiol.* **31**(Suppl. 1), 45–49. [discussion 50–51]

May-Newman, K. & Yin, F. C. 1998 A constitutive law for mitral valve tissue. *J. Biomech. Eng.* **120**, 38–47.

Miller, G. E. & Marcotte, H. 1987 Computer simulation of human mitral valve mechanics and motion. *Comput. Biol. Med.* **17**, 305–319. (doi:10.1016/0010-4825(87)90020-5)

Nielsen, S. L., Nygaard, H., Fontaine, A. A., Hasenkam, J. M., He, S., Andersen, N. T. & Yoganathan, A. P. 1999 Chordal force distribution determines systolic mitral leaflet configuration and severity of functional mitral regurgitation. *J. Am. Coll. Cardiol.* **33**, 843–853. (doi:10.1016/S0735-1097(98)00627-5)

Olson, L. J., Subramanian, R., Ackermann, D. M., Orszulak, T. A. & Edwards, W. D. 1987 Surgical pathology of the mitral valve: a study of 712 cases spanning 21 years. *Mayo Clin. Proc.* **62**, 22–34.

Perloff, J. K. & Roberts, W. C. 1972 The mitral apparatus. Functional anatomy of mitral regurgitation. *Circulation* **46**, 227–239.

Pohost, G. M. *et al.* 1975 The echocardiogram of the anterior leaflet of the mitral valve. Correlation with hemodynamic and cineroentgenographic studies in dogs. *Circulation* **51**, 88–97.

Priola, D. V., Fellows, C., Moorehouse, J. & Sanchez, R. 1970 Mechanical activity of canine mitral valve *in situ*. *Am. J. Physiol.* **219**, 1647–1651.

Quick, D. W., Kunzelman, K. S., Kneebone, J. M. & Cochran, R. P. 1997 Collagen synthesis is upregulated in mitral valves subjected to altered stress. *ASAIO J.* **43**, 181–186. (doi:10.1097/00002480-199705000-00011)

Quick, D., Kunzelman, K., Hata, M., Hegge, J., Rahko, P., Weigl, T. & Cochran, R. 2004 Effect of infarction and ACE inhibitors on the mitral valve. *J. Ariz. Nev. Acad. Sci.* **37**, 94–99. (doi:10.2181/1533-6085(2004)037<0094:EOIAAI>2.0.CO;2)

Redaelli, A., Guadagni, G., Fumero, R., Maisano, F. & Alfieri, O. 2001 A computational study of the hemodynamics after 'edge-to-edge' mitral valve repair. *J. Biomech. Eng.* **123**, 565–570. (doi:10.1115/1.1408938)

Reimink, M. S., Kunzelman, K. S., Verrier, E. D. & Cochran, R. P. 1995 The effect of anterior chordal replacement on mitral valve function and stresses. A finite element study. *ASAIO J.* **41**, M754–M762.

Reimink, M. S., Kunzelman, K. S. & Cochran, R. P. 1996 The effect of chordal replacement suture length on function and stresses in repaired mitral valves: a finite element study. *J. Heart Valve Dis.* **5**, 365–375.

Roberts, W. C. 1983 Morphologic features of the normal and abnormal mitral valve. *Am. J. Cardiol.* **51**, 1005–1028. (doi:10.1016/S0002-9149(83)80181-7)

Rubenstein, J. J., Pohost, G. M., Dinsmore, R. E. & Harthorne, J. W. 1975 The echocardiographic determination of mitral valve opening and closure. Correlation with hemodynamic studies in man. *Circulation* **51**, 98–103.

Rusted, I. E., Scheifley, C. H. & Edwards, J. E. 1952 Studies of the mitral valve. I. Anatomic features of the normal mitral valve and associated structures. *Circulation* **6**, 825–831.

Sacks, M. S., He, Z., Baijens, L., Wanant, S., Shah, P., Sugimoto, H. & Yoganathan, A. P. 2002 Surface strains in the anterior leaflet of the functioning mitral valve. *Ann. Biomed. Eng.* **30**, 1281–1290. (doi:10.1114/1.1529194)

Salgo, I. S., Gorman III, J. H., Gorman, R. C., Jackson, B. M., Bowen, F. W., Plappert, T., St John Sutton, M. G. & Henry Edmunds, L. 2002 Effect of annular shape on

leaflet curvature in reducing mitral leaflet stress. *Circulation* **106**, 711–717. (doi:10.1161/01.CIR.0000025426.39426.83)

Salisbury, P. F., Cross, C. E. & Rieben, P. A. 1963 Chorda tendinea tension. *Am. J. Physiol.* **205**, 385–392.

Stein, P. D. & Sabbah, H. N. 1978 Accentuation of heart sounds in anemia: an effect of blood viscosity. *Am. J. Physiol.* **235**, H664–H669.

Votta, E., Maisano, F., Soncini, M., Redaelli, A., Montevecchi, F. M. & Alfieri, O. 2002 3-D computational analysis of the stress distribution on the leaflets after edge-to-edge repair of mitral regurgitation. *J. Heart Valve Dis.* **11**, 810–822.

Waller, B. F., Morrow, A. G., Maron, B. J., Del Negro, A. A., Kent, K. M., McGrath, F. J., Wallace, R. B., McIntosh, C. L. & Roberts, W. C. 1982 Etiology of clinically isolated, severe, chronic, pure mitral regurgitation: analysis of 97 patients over 30 years of age having mitral valve replacement. *Am. Heart J.* **104**, 276–288. (doi:10.1016/0002-8703(82)90204-6)

Yun, K. L. & Miller, D. C. 1991 Mitral valve repair versus replacement. *Cardiol. Clin.* **9**, 315–327.